Photonic Dissipation Control for Kerr Soliton Generation in Strongly Raman-Active Media

Zheng Gong,[1] Ming Li,[2] Xianwen Liu,[1] Yuntao Xu,[1] Juanjuan Lu,[1] Alexander Bruch,[1] Joshua B. Surya,[1] Changling Zou,[1,2] and Hong X. Tang[1,*]

[1]Department of Electrical Engineering, Yale University, New Haven, Connecticut 06511, USA

[2]Department of Optics and Optics Engineering, University of Science and Technology of China, Hefei, Anhui 230026, China

(Received 17 March 2020; accepted 28 September 2020; published 28 October 2020)

Microcavity solitons enable miniaturized coherent frequency comb sources. However, the formation of microcavity solitons can be disrupted by stimulated Raman scattering, particularly in the emerging crystalline microcomb materials with high Raman gain. Here, we propose and implement dissipation control—tailoring the energy dissipation of selected cavity modes—to purposely raise or lower the threshold of Raman lasing in a strongly Raman-active lithium niobate microring resonator and realize on-demand soliton mode locking or Raman lasing. Numerical simulations are carried out to confirm our analyses and agree well with experiment results. Our work demonstrates an effective approach to address strong stimulated Raman scattering for microcavity soliton generation.

DOI: 10.1103/PhysRevLett.125.183901

Microcavity solitons [1] are miniaturized coherent frequency comb sources that have promising applications that range from time-frequency metrology to advanced communications [2]. However, their formation inside the cavity can be strongly perturbed by stimulated Raman scattering (SRS) [3,4] originating from inelastic scattering of photons by lattice phonon modes [5]. When the pump field energy is above a threshold level, Raman lasing is initiated and interferes with the four-wave mixing process [6–9], disrupting soliton formation [3]. This is of particular concern in comb materials with strong Raman gain such as silicon [6], diamond [10], GaP [11], AlN [9,12], and lithium niobate (LN) [13]. The latter three are emerging crystalline materials that hold great potential for on-chip comb self-referencing [11,14–17] due to their simultaneous χ^3 and χ^2 optical nonlinearities.

Methods to mitigate SRS include reducing the microresonator size [3] and orientating field polarization along the proper crystal axis [18], which serve to reduce the spectral overlap between soliton-forming modes and dominating Raman gain. However, these solutions impose limits on device geometry and may affect the extent of dispersion control. On the other hand, optical microresonators can also be considered an "open" system driven by an external field, while dissipating energy either through the cavity's internal losses or by coupling to external waveguides. Thus, SRS could also be manipulated from the perspective of dissipation control through the adjustment of the external coupling rates of the Raman mode with respect to soliton-forming cavity modes. Along this line of thinking, auxiliary microrings [19], engineered pulley waveguide couplers [20], and scattering centers [19,21,22] have been proposed to modify the loss of cavity modes.

In this Letter, we demonstrate dissipation control in the photonic domain using a microresonator formed on thin film LN, a highly Raman-active material, to suppress Raman lasing and allow soliton comb generation. By exploiting a self-interference coupling structure, the external coupling rates among cavity modes are controlled to raise the Raman lasing intracavity pump mode threshold energy above the one needed for a single soliton, thus securing the soliton state. An analytical model is established to estimate and compare the intracavity pump mode threshold energies of the Raman lasing and Kerr soliton state. Also, numerical simulations are carried out to study the cavity dynamics. Both analytical and numerical results are consistent with experimental observations.

A conceptual representation of dissipation control in a Raman-active optical microresonator is shown in Fig. 1. The μth soliton-forming mode dissipates energy through intrinsic loss channels at $\kappa_{i,\mu}$ and the external coupling waveguide at $\kappa_{e,\mu}$. In addition to four-wave mixing within the soliton-forming mode family, a strong Raman effect will also transfer pump mode energy to the Stokes modes, which could lead to Raman lasing but can be suppressed by enhancing $\kappa_{e,R}$. Specifically, we consider the first-order lasing threshold of the dominant Raman mode in a microring [12], defined as the minimum required intracavity pump mode energy to initiate the Raman lasing and given by (see the Supplemental Material [23])

$$\varepsilon_{R,\mathrm{th}} = \frac{\hbar\omega_p \gamma_R \kappa_R}{4g_R^2}\left[1+\left(\frac{2\delta_R}{\gamma_R}\right)^2\right], \tag{1}$$

where γ_R is the full-width at half-maximum (FWHM) of the Raman gain, $\kappa_R = \kappa_{i,R} + \kappa_{e,R}$ is the total cavity decay rate

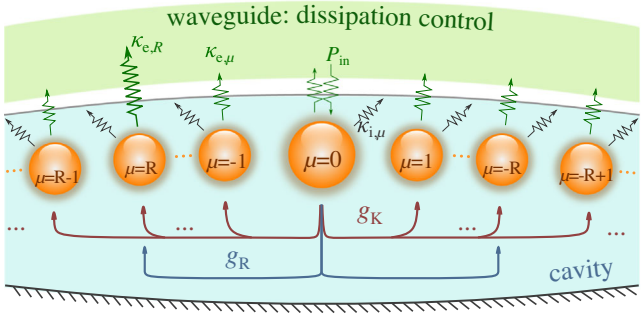

FIG. 1. Bubbles: Soliton-forming modes in the optical microresonator (blue-colored region), numbered with respect to the pump mode. Red arrowed lines: Kerr nonlinear coupling with a rate of g_k. Blue arrowed lines: First SRS from the pump mode to the Stokes mode R with a rate of g_R and subsequent anti-SRS at mode $-R$. [5]. Gray coils: Cavity intrinsic dissipation rate ($\kappa_{i,\mu}$). Green coils: Cavity-waveguide coupling rate ($\kappa_{e,\mu}$).

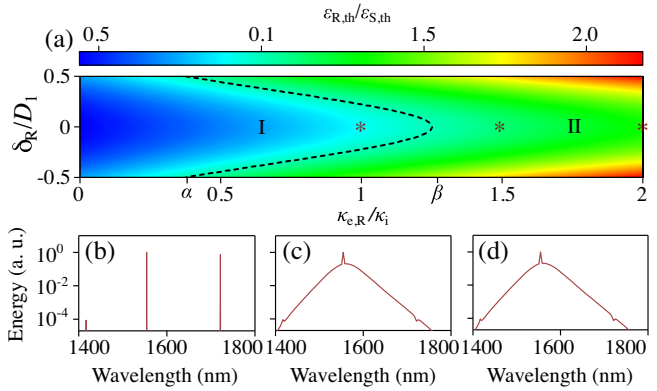

FIG. 2. (a) Threshold ratio $\varepsilon_{R,\mathrm{th}}/\varepsilon_{S,\mathrm{th}}$ as the Raman mode detuning δ_R/D_1 and external coupling ratio $\kappa_{e,R}/\kappa_i$ are varied. The dashed curve separates the $\varepsilon_{R,\mathrm{th}} < \varepsilon_{S,\mathrm{th}}$ (I) and $\varepsilon_{R,\mathrm{th}} > \varepsilon_{S,\mathrm{th}}$ (II) regimes. (b)–(d) Simulated intracavity spectra for Raman lasing and soliton combs at $\delta_R/D_1 = 0$ and $\kappa_{e,R}/\kappa_i = 1$, 1.5, and 2 marked by asterisks in (a), respectively. Insets show the temporal profiles. For (a)–(d), $\kappa_i/(2\pi) = \kappa_e/(2\pi) = 235$ MHz, $D_2/\kappa_i = 8.6 \times 10^{-2}$. The soliton self-frequency shifts in (c),(d) are 0.9 THz.

of the Stokes mode ($\mu = R$ in Fig. 1), g_R denotes the Raman coupling rate, and $\delta_R = \Omega_R - (\omega_p - \omega_R)$ represents the Raman gain detuning with ω_p and ω_R denoting pump and Stokes light angular frequencies. Note that the onset of the first-order Raman lasing will result in a clamped pump mode energy at $\varepsilon_{R,\mathrm{th}}$.

Under pure Kerr effect and ignoring higher-order dispersion, the minimal intracavity pump mode energy required by a single soliton with an FWHM of γ_S can be approximated as [1]

$$\varepsilon_{S,\mathrm{th}} \simeq \frac{\hbar\omega_p D_2}{4g_K}\left[1 + 2\left(\frac{\kappa D_1}{\gamma_S D_2}\right)^2\right], \tag{2}$$

where D_1 represents the free spectral range ($D_1 = 2\pi\mathrm{FSR}$), $D_2 > 0$ denotes the second dispersion, and $g_K = (\hbar\omega_0^2 c n_2)/(n_0^2 V_{\mathrm{eff}})$ is the Kerr nonlinear coupling rate, with c, n_2, n_0, and V_{eff} being the speed of light in vacuum, nonlinear refractive index, effective refractive index, and mode volume, respectively [1]. In this analytical model, a single $\kappa = \kappa_e + \kappa_i$ is used to describe the total cavity decay rate for all the optical modes, while mode-dependent coupling rates are included in the numerical model [23]. The leading term in Eq. (2) represents the energy of the frequency component at ω_p of the pulse, and the second term signifies the energy of the continuous wave background.

Raman lasing can be suppressed by raising the Raman gain detuning δ_R [3], causing an increase in $(\delta_R/\gamma_R)^2$ and threshold. However, adjusting δ_R alone imposes a lower limit on the soliton comb repetition rate [2,3]. On the other hand, if one manages to increase $\kappa_{e,R}$ by engineering the cavity's external coupling configuration, then the restraint on the ring geometry will be largely relaxed.

To illustrate raising $\varepsilon_{R,\mathrm{th}}$ above $\varepsilon_{S,\mathrm{th}}$ with increased $\kappa_{e,R}$, the calculated $\varepsilon_{R,\mathrm{th}}/\varepsilon_{S,\mathrm{th}}$ under different Raman detunings and external coupling rates are presented in Fig. 2. Here, we attempt to secure a single soliton, with a target FWHM of 6.5 THz as an example, in a cavity where the Raman gain FWHM is larger than the microring FSR, with $\gamma_R/D_1 = 1.3$, chosen to reflect our actual device parameters. Both the Raman and Kerr coefficients are set using corresponding literature values of LN. To gain insight into the complex dynamics of the coupled nonlinear processes, only $\kappa_{e,R}$ of the Stokes mode is varied while κ_i and κ_e remain unchanged for the other modes, and the calculation of $\varepsilon_{S,\mathrm{th}}$ based on Eq. (2) ignores the variation of $\kappa_{e,R}$ at the Stokes mode, which is far away from the pump mode. The numerical model presented later [Fig. 2(b)–2(d)] incorporates mode-dependent coupling rates, and the main conclusions drawn from our simplified model remain valid.

Fig. 2(a) delineates separate regimes for Raman threshold being lower or higher than the soliton state's (I/II). For a small external coupling rate at the Stokes mode ($\kappa_{e,R}/\kappa_i < \alpha$), the Raman lasing threshold is always lower than that of the soliton state, even if the Raman gain peak is optimally detuned from adjacent soliton-forming modes (in the middle between two modes). Here, $\alpha = 4g_R^2\varepsilon_{S,\mathrm{th}}/[\hbar\omega_p\kappa_i(\gamma_R + D_1^2/\gamma_R)] - 1$ is a material- and device-dependent dimensionless parameter. At an increased Stokes mode external coupling rate ($\alpha < \kappa_{e,R}/\kappa_i < \beta = [1 + (D_1/\gamma_R)^2]\alpha$), the Raman lasing threshold can be elevated above the soliton state's when there is sufficient detuning between the Raman gain peak and adjacent modes.

By further increasing $\kappa_{e,R}$ ($\kappa_{e,R}/\kappa_i > \beta$), the soliton state is favored over Raman lasing for all possible Raman–Stokes detunings. Numerical simulations carried out at several representative locations marked in the parameter space of Fig. 2(a) suggest that the single soliton state can be

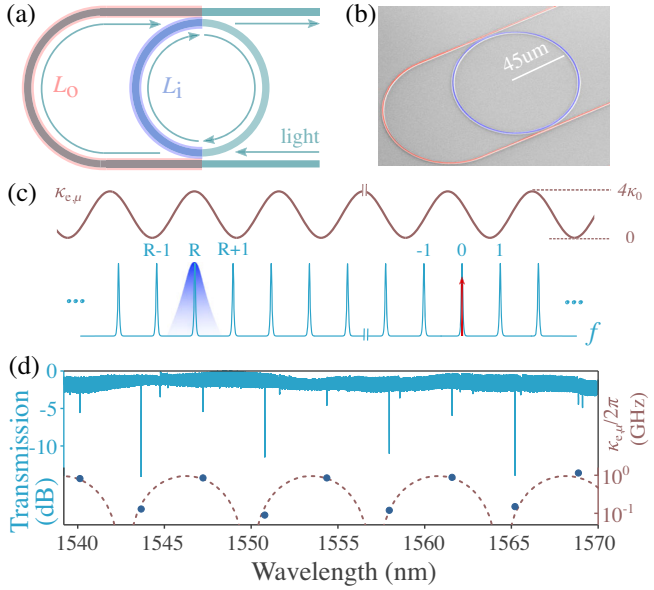

FIG. 3. (a) Schematic of a self-interferenced microring. Purple (pink) shaded line: The inner (outer) arm of the interferometer, with its length denoted as $L_{i(o)}$. (b) False-color SEM of the U-ring. (c) Schematic illustration of modulated $\kappa_{e,\mu}$ (brown line) to suppress Raman lasing. Cyan peaks: soliton-forming modes. Red arrow marks the pump mode. Blue shaded profile: the Raman gain. (d) Cyan line: measured transverse-electric transmission of (b). Dashed brown line: predicted κ_e curve from Eq. (3). Cyan dots: extracted $\kappa_{e,\mu}$ from the measured transmission by fitting the linewidths of the resonances.

maintained, even when the Raman gain peak overlaps the Stokes mode. As examples, the simulated intracavity spectra for $\varepsilon_{R,\mathrm{th}}/\varepsilon_{S,\mathrm{th}} = 0.9$, 1.1, and 1.3 are presented in Figs. 2(b)–2(d).

To implement the dissipation control concept described above, it is critical that the external coupling rate of the Raman modes can be engineered. For the purpose of tuning the external coupling rates of selected modes, the photonics community has established approaches that include the use of a pulley waveguide [20,31,32] and auxiliary microring [19,33,34]. Here we adopt a self-interference structure [Fig. 3(a)] that offers high dynamic tuning of κ_e, integrability with local heater or electrode for fine tuning [35,36], as well as extendability for the suppression of multiple Raman lines. The scanning electron micrograph (SEM) image of our device is shown in Fig. 3(b), where the external waveguide couples twice with the microring (referred to U-ring hereafter). The net external coupling rate of μth mode $\kappa_{e,\mu}$ is given by [23]

$$\kappa_{e,\mu} = 2\kappa_0(1 + \cos\phi_\mu), \tag{3}$$

where κ_0 is the coupling rate at each of the two identical microring-waveguide couplers, and $\phi_\mu = [\omega(\mu)/c](L_o n_o - L_i n_i)$ is the mode-dependent phase difference between the two arms with $L_{i(o)}$ and $n_{i(o)}$ denoting the length and effective index of the inner (outer) arm of the μth mode. The schematic in Fig. 3(c) illustrates the modulation of external coupling rates around the Stokes mode $\mu = R$. The Stokes mode can be aligned to the peak of κ_e curve by using a modulation period larger than the Raman gain FWHM and selecting proper pump wavelength. In the experiment [Fig. 3(d)], we used a fast modulation ($L_o \approx 2L_i$) to provide a higher probability of finding a suitable pump mode within the erbium-doped fiber amplifier bandwidth.

Our microring resonator is patterned from a z-cut LN thin film [37,38] that exhibits anomalous dispersion $D_2/(2\pi) \approx 20$ MHz and possesses strong Raman gain $g_R/g_k \approx 1.3 \times 10^6$ with a linewidth of $\gamma_R \approx 1.3D_1$. Without dissipation control, the SRS is dominant and leads to first-order Raman lasing at the mode $\mu = -42$, corresponding to the dominant $E(\mathrm{LO}_8)$ Raman mode [12,23]. The transmission of the U-ring is presented in Fig. 3(d), where the extracted external coupling rates are plotted against the values predicted by Eq. (3) with $\kappa_0/(2\pi) = 1.1\kappa_i/(2\pi) = 240$ MHz and a modulation period of 2.02 FSR. To estimate $\varepsilon_{S,\mathrm{th}}$, we consider a sech^2-weighted external coupling rate $\kappa_e = [\sum \mathrm{sech}^2(\mu/N)\kappa_{e,\mu}]/[\sum \mathrm{sech}^2(\mu/N)]$ that factors in $\kappa_{e,\mu}$ being modulated across the soliton-forming modes and phenomenologically represents a collective soliton external coupling rate where $N \cdot \mathrm{FSR}$ indicates the bandwidth of interest. Under this simplification, $\varepsilon_{S,\mathrm{th}}$ can be estimated by Eq. (2) and 1.2 times higher than the numerically simulated value considering mode-dependent external coupling rates [23].

To suppress Raman lasing in favor of soliton generation, we chose to pump a TE_{00} mode at 1554.4 nm whose Stokes mode sees a high external coupling rate $\kappa_{e,R} = 3.7\kappa_0$ as inferred from Fig. 3(d). The estimated Raman lasing threshold is raised above the targeted soliton state threshold by $\varepsilon_{R,\mathrm{th}}/\varepsilon_{S,\mathrm{th}} = 1.1$. As expected, the single soliton comb can be successfully generated in the experiment by scanning the pump along the red side of the resonance [14,37] until the soliton step shows up [Fig. 4(b) inset]. The recorded output spectrum is shown in Fig. 4(b), in which each comb line power is modulated by its external coupling rate $P_{S,\mu} \propto \varepsilon_{S,\mu}\kappa_{e,\mu}$, where $\varepsilon_{S,\mu}$ is the μth mode's intracavity energy. Assuming that the intracavity mode energy $\varepsilon_{S,\mu}$ maintains a $sech^2$-profile, $\kappa_{e,\mu}$ can be separately extracted from the measured spectrum [Fig. 4(a)]. The numerical simulation shown in Fig. 4(e) verifies that the single soliton can be obtained under this configuration. It is notable that, in a time-domain picture, the intracavity soliton couples to the U-arm and is subsequently fed back to the microring every round-trip, introducing a weak feedback pulse of less than 1% intensity of the main pulse [inset of Fig. 4(e)]. This time-domain picture is captured in the frequency domain by the modulated $\kappa_{e,\mu}$ [Fig. 4(d)]. Here a dip [Fig. 4(e) inset] is observed due to the out-of-phase delay introduced by the chosen path difference $L_o n_o - L_i n_i$.

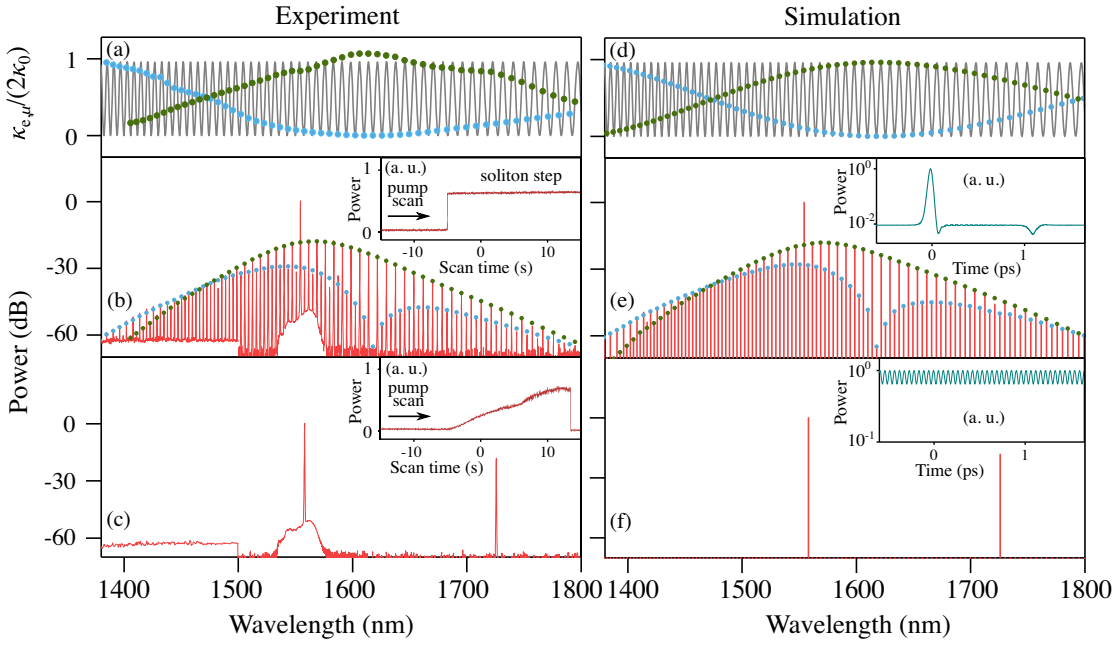

FIG. 4. (a) External coupling rate $\kappa_{e,\mu}$, marked alternately with cyan or green dots, are extracted from the corresponding cyan or green dotted curve tracing the measured comb line powers in panel (b). The gray line in the background is the predicted continuous κ_e curve. The deviation of the extracted external couplings from the theoretically calculated may be ascribed to local mode crossings that affect the extraction of $\kappa_{e,\mu}$. (b) The measured and normalized soliton comb output spectrum with an FSR of ~445.7 GHz under on-chip pump power of 200 mW. Cyan or green dotted curve: Spectral envelope. Inset: Comb power under red-to-blue pump scan (0.25 GHz/s). (c) The measured and normalized first-order Raman lasing spectrum. Inset: Stokes light power trace under the same scan for the inset of (b). (d) Cyan or green dots: $\kappa_{e,\mu}$ for the simulation, calculated by Eq. (3) with $\kappa_0/(2\pi) = 240$ MHz and $c/(L_o n_o - L_i n_i) = 900$ GHz. Gray line is the same to (a). (e),(f) The simulated and normalized soliton comb and Raman lasing spectra on the output waveguide. Cyan or green dotted curve: Spectral envelope imposed by $\kappa_{e,\mu}$ (cyan or green dots) in (d). Insets: Intracavity temporal profiles. The time interval between the soliton and the feedback pulse is determined by the path difference $(L_o n_o - L_i n_i)/c = 1.1$ ps.

The U-ring switches to Raman lasing, with no solitons observed, when pumped at 1558 nm (one FSR away from the previous setting). At this detuning, the Stokes mode sees a smaller $\kappa_{e,R} = 0.4\kappa_0$ [Fig. 3(d)]. As a result, the lasing threshold $\varepsilon_{R,\mathrm{th}}$ drops by a factor of 3.6 and leads to an estimated $\varepsilon_{R,\mathrm{th}}/\varepsilon_{S,\mathrm{th}} = 0.3$. The recorded Raman lasing output spectrum is displayed in Fig. 4(c). Only the Stokes output power was recorded in the power-time trace with no soliton steps observed [Fig. 4(c) inset]. The numerically simulated output spectrum shown in Fig. 4(f) confirms Raman lasing without the formation of the Kerr soliton.

In conclusion, the use of dissipation control in a Raman-active microcavity to suppress Raman lasing for soliton generation was demonstrated. Theoretical analyses and numerical simulations suggest that the competition between intracavity Raman lasing and soliton formation can be controlled by systematically engineering the external coupling rates, where the final steady state relies on which state has a lower threshold pump mode energy. The concept is implemented via a self-interference coupling structure. By pumping different modes along the modulation curve, soliton mode locking and Raman lasing can be steered on demand in a single device. This design concept can be extended to more complex coupling structures to suppress multiple Raman gain lines or a stronger Raman effect [23]. Our work provides guidance on how to overcome challenges related to the competition between intracavity Raman lasing and soliton formation from the perspective of dissipation control and could inspire future studies on regulating intracavity dynamics where multiple nonlinear processes are present.

We acknowledge funding support from Defense Advanced Research Projects Agency. H. X. T. acknowledges support from a Packard Fellowship in Science and Engineering. The authors thank Yong Sun, Sean Rinehart, Kelly Woods, and Michael Rooks for assistance in device fabrication.

*Corresponding author.
hong.tang@yale.edu

[1] T. Herr, V. Brasch, J. D. Jost, C. Y. Wang, N. M. Kondratiev, M. L. Gorodetsky, and T. J. Kippenberg, Nat. Photonics **8**, 145 (2014).
[2] A. L. Gaeta, M. Lipson, and T. J. Kippenberg, Nat. Photonics **13**, 158 (2019).
[3] Y. Okawachi, M. Yu, V. Venkataraman, P. M. Latawiec, A. G. Griffith, M. Lipson, M. Lončar, and A. L. Gaeta, Opt. Lett. **42**, 2786 (2017).

[4] Y. Wang, M. Anderson, S. Coen, S. G. Murdoch, and M. Erkintalo, Phys. Rev. Lett. **120**, 053902 (2018).

[5] G. Agrawal, in *Nonlinear Fiber Optics (Fifth Edition)*, Optics and Photonics, edited by G. Agrawal (Academic Press, Boston, 2013), pp. 295–352.

[6] A. G. Griffith, M. Yu, Y. Okawachi, J. Cardenas, A. Mohanty, A. L. Gaeta, and M. Lipson, Opt. Express **24**, 13044 (2016).

[7] X. Liu, C. Sun, B. Xiong, L. Wang, J. Wang, Y. Han, Z. Hao, H. Li, Y. Luo, J. Yan, T. Wei, Y. Zhang, and J. Wang, ACS Photonics **5**, 1943 (2018).

[8] H. Choi and A. M. Armani, Opt. Lett. **43**, 2949 (2018).

[9] H. Jung, Z. Gong, X. Liu, X. Guo, C. ling Zou, and H. X. Tang, Opt. Express **27**, 22246 (2019).

[10] P. Latawiec, V. Venkataraman, M. J. Burek, B. J. M. Hausmann, I. Bulu, and M. Lončar, Optica **2**, 924 (2015).

[11] D. J. Wilson, K. Schneider, S. Hoenl, M. Anderson, T. J. Kippenberg, and P. Seidler, Nat. Photonics **14**, 57 (2020).

[12] X. Liu, C. Sun, B. Xiong, L. Wang, J. Wang, Y. Han, Z. Hao, H. Li, Y. Luo, J. Yan, T. Wei, Y. Zhang, and J. Wang, Optica **4**, 893 (2017).

[13] M. Yu, Y. Okawachi, R. Cheng, C. Wang, M. Zhang, A. L. Gaeta, and M. Lončar, in *Conference on Lasers and Electro-Optics* (Optical Society of America, San Jose, 2019), p. JTh5A.2.

[14] Y. He, Q.-F. Yang, J. Ling, R. Luo, H. Liang, M. Li, B. Shen, H. Wang, K. Vahala, and Q. Lin, Optica **6**, 1138 (2019).

[15] H. Jung, C. Xiong, K. Y. Fong, X. Zhang, and H. X. Tang, Opt. Lett. **38**, 2810 (2013).

[16] A. W. Bruch, X. Liu, J. B. Surya, C.-L. Zou, and H. X. Tang, Optica **6**, 1361 (2019).

[17] Z. Gong, A. Bruch, M. Shen, X. Guo, H. Jung, L. Fan, X. Liu, L. Zhang, J. Wang, J. Li, J. Yan, and H. X. Tang, Opt. Lett. **43**, 4366 (2018).

[18] M. Yu, Y. Okawachi, R. Cheng, C. Wang, M. Zhang, A. L. Gaeta, and M. Lončar, Light Sci. Appl. **9**, 9 (2020).

[19] Y. Jestin, A. B. Matsko, A. A. Savchenkov, and L. Maleki, Proc. SPIE Int. Soc. Opt. Eng. **7194**, 139 (2009).

[20] Y. Zheng, C. Sun, B. Xiong, L. Wang, J. Wang, Y. Han, Z. Hao, H. Li, and Y. Luo, in *Conference on Lasers and Electro-Optics* (Optical Society of America, San Jose, 2019), p. JTu2A.90.

[21] M. L. Gorodetsky, A. D. Pryamikov, and V. S. Ilchenko, J. Opt. Soc. Am. B **17**, 1051 (2000).

[22] T. J. Kippenberg, A. L. Tchebotareva, J. Kalkman, A. Polman, and K. J. Vahala, Phys. Rev. Lett. **103**, 027406 (2009).

[23] See Supplemental Material, which includes Refs. [24–30], at http://link.aps.org/supplemental/10.1103/PhysRevLett.125.183901 for theoretical derivation, numerical simulation, experiment setup, and device characterization.

[24] Q.-F. Yang, X. Yi, K. Y. Yang, and K. Vahala, Optica **3**, 1132 (2016).

[25] M. Karpov, H. Guo, A. Kordts, V. Brasch, M. H. P. Pfeiffer, M. Zervas, M. Geiselmann, and T. J. Kippenberg, Phys. Rev. Lett. **116**, 103902 (2016).

[26] A. Ridah, P. Bourson, M. D. Fontana, and G. Malovichko, J. Phys. Condens. Matter **9**, 9687 (1997).

[27] J. Heebner, R. Grover, T. Ibrahim, and T. Ibrahim, *Optical Microresonators: Theory, Fabrication, and Applications*, Optical Sciences 138 (Springer, New York, 2008).

[28] T. Herr, V. Brasch, J. D. Jost, I. Mirgorodskiy, G. Lihachev, M. L. Gorodetsky, and T. J. Kippenberg, Phys. Rev. Lett. **113**, 123901 (2014).

[29] E. S. Lamb, D. R. Carlson, D. D. Hickstein, J. R. Stone, S. A. Diddams, and S. B. Papp, Phys. Rev. Applied **9**, 024030 (2018).

[30] H. Guo, M. Karpov, E. Lucas, A. Kordts, M. H. P. Pfeiffer, V. Brasch, G. Lihachev, V. E. Lobanov, M. L. Gorodetsky, and T. J. Kippenberg, Nat. Phys. **13**, 94 (2017).

[31] E. S. Hosseini, S. Yegnanarayanan, A. H. Atabaki, M. Soltani, and A. Adibi, Opt. Express **18**, 2127 (2010).

[32] G. Moille, Q. Li, T. C. Briles, S.-P. Yu, T. Drake, X. Lu, A. Rao, D. Westly, S. B. Papp, and K. Srinivasan, Opt. Lett. **44**, 4737 (2019).

[33] S. A. Miller, Y. Okawachi, S. Ramelow, K. Luke, A. Dutt, A. Farsi, A. L. Gaeta, and M. Lipson, Opt. Express **23**, 21527 (2015).

[34] X. Xue, Y. Xuan, P.-H. Wang, Y. Liu, D. E. Leaird, M. Qi, and A. M. Weiner, Laser Photonics Rev. **9**, L23 (2015).

[35] L. Chen, N. Sherwood-Droz, and M. Lipson, Opt. Lett. **32**, 3361 (2007).

[36] S. Wan, R. Niu, H.-L. Ren, C.-L. Zou, G.-C. Guo, and C.-H. Dong, Photonics Res. **6**, 681 (2018).

[37] Z. Gong, X. Liu, Y. Xu, M. Xu, J. B. Surya, J. Lu, A. Bruch, C. Zou, and H. X. Tang, Opt. Lett. **44**, 3182 (2019).

[38] J. Lu, J. B. Surya, X. Liu, A. W. Bruch, Z. Gong, Y. Xu, and H. X. Tang, Optica **6**, 1455 (2019).